n-Type Transparent Conducting Films of Small Molecule and Polymer Amine Doped Single-Walled Carbon Nanotubes

Kevin S. Mistry,[†,‡] Brian A. Larsen,[†] Jeremy D. Bergeson,[†] Teresa M. Barnes,[†] Glenn Teeter,[†] Chaiwat Engtrakul,[†] and Jeffrey L. Blackburn[†,*]

[†]National Renewable Energy Laboratory, Golden, Colorado 80401, United States, and [‡]Department of Physics, University of Colorado, Boulder, Colorado 80309, United States

ABSTRACT In this report, we investigate the electrical and optical properties of thin conducting films of SWNTs after treatment with small molecule and polymeric amines. Among those tested, we find hydrazine to be the most effective n-type dopant. We use absorbance, Raman, X-ray photoelectron, and nuclear magnetic resonance spectroscopies on thin conducting films and opaque buckypapers treated with hydrazine to study fundamental properties and spectroscopic signatures of n-type SWNTs and compare them to SWNTs treated with nitric acid, a well-characterized p-type dopant. We find that hydrazine physisorbs to the surface of semiconducting and metallic SWNTs and injects large electron concentrations, raising the Fermi level as much as 0.7 eV above that of intrinsic SWNTs. Hydrazine-treated transparent SWNT films display sheet resistances nearly as low as p-type nitric-acid-treated films at similar optical transmittances, demonstrating their potential for use in photovoltaic devices as low work function transparent *electron-collecting* electrodes.

KEYWORDS: single-walled carbon nanotubes · photovoltaics · doping · n-type · transparent conductor · amine · thin films

Single-walled carbon nanotubes (SWNTs) can be either metallic or semiconducting, depending on their chiral index,[1] but can be doped with high electron or hole concentrations by charge transfer reactions with adsorbed molecules, such that both types of nanotubes exhibit metallic-like behavior. Controllable p- and n-type doping of SWNT films can be used to enable many different technologies, such as field effect transistors, light-emitting diodes, and solar cells.[2−6] Because most p-type dopants for SWNTs are environmentally stable, they have been studied in greater detail and used in far more applications than their n-type counterparts, which tend to be less stable. As a result, further studies on the fundamental properties, spectroscopic signatures, and potential applications of n-type SWNTs are needed.

Although the technological application of n-type SWNTs thus far has been primarily relegated to single-tube field effect transistors, other technologies could significantly benefit from macroscopic n-type SWNT networks. For example, thin conducting films (TCFs) of SWNTs are seen as a possible replacement for traditional transparent conducting oxide (TCO) films in photovoltaic (PV) devices, but first they must achieve comparable sheet resistances and optical transmittance over a large range of wavelengths.[2,3,7] p-Type SWNT TCFs have been incorporated into photovoltaic devices as hole-collecting electrodes,[2,3,7] but evaporated metal electrodes still tend to be used as the electron-collecting electrode, negating some of the intended benefits of the solution-processed SWNT TCF. However, the amphoteric nature of SWNTs implies that SWNT networks could be used to collect both types of carriers. Low work function n-type SWNT TCFs could also enable flexible, solution-processed organic light-emitting diodes (OLEDs), in which a SWNT cathode and anode are used to *inject* both types of carriers. Recent work has demonstrated the use of SWNT networks with equivalent work functions as both cathode and anode in a light-emitting electrochemical cell (LEC).[8] In LECs, the diffusion of mobile ions alleviates the need for a low work function cathode, but also leads to a much slower response time than is typical for OLEDs. Finally, other recent studies report the formation of highly efficient p−n junctions on individual SWNTs that are chemically doped[9] or electrostatically gated[10] p- and n-type on either end, but translating such single-tube successes into macroscopic all-SWNT p−n junction photovoltaic devices will be challenging.

n-Type chemical doping of SWNTs has been performed by two general approaches—treatment with alkali metals

* Address correspondence to jeffrey.blackburn@nrel.gov.

Received for review January 7, 2011 and accepted March 9, 2011.

Published online March 09, 2011
10.1021/nn200076r

and adsorption/intercalation of small molecules or polymers. Alkali metal doping relies on either vapor transport of the metal into a SWNT network or intercalation of metal ions in aprotic solvents such as THF or DMSO.[11,12] In some cases, doping by alkali metals has been observed to introduce irreversible structural defects as observed by an increased D band in Raman spectra.[13] The majority of molecular n-type SWNT dopants consist of amine-containing molecules or polymers, although other organic dopants have been utilized.[14,15] Small molecule amines, such as hydrazine, and amine-containing polymers, such as polyethylenimine (PEI), have been used to create n-type single-tube or sparse-network field effect transistors.[16,17] Other work has used hydrazine to disperse nanotubes through electrostatic repulsions,[18] similar to the case of alkali-metal saturated organic solvents mentioned above.[11] To our knowledge, no groups have applied n-type doping strategies to thin, optically transparent SWNT networks. Furthermore, fundamental spectroscopic studies of n-type SWNTs are relatively scarce in the literature, motivating the need for more detailed investigations.

In this study, we investigate the effects of several amines on thin SWNT films to find an effective n-type dopant for SWNT TCFs. On the basis of conductivity and optical transparency, we determine hydrazine (N_2H_4) to be more effective than methylamine, ethylenediamine, and polyethylenimine. Then, using hydrazine as a case study, we use a combination of Raman spectroscopy, X-ray photoelectron spectroscopy (XPS), and nuclear magnetic resonance (NMR) to investigate the mechanisms underlying the interactions of amines with SWNT networks. Using a range of macroscopic samples, from transparent films to opaque buckypapers, allows us to correlate a variety of doping-induced spectroscopic modifications to the excellent transport properties obtained by hydrazine doping. Previous work on the doping effects of hydrazine on SWNTs has focused on single-tube field effect transistors (FETs).[16,19] In contrast to studies of single-tube FETs where it is difficult to decouple the carrier density injected into the nanotube from modification of the nanotube/contact junction by the dopant,[16,20] we unambiguously find physisorbed hydrazine to be an effective n-type dopant of SWNTs when used in an inert environment. Moreover, we find that N_2H_4 can produce films with nearly the same sheet resistance (at a given transparency) as p-doped HNO_3-treated films due to the injection of extremely high electron densities into both semiconducting and metallic SWNTs. These results serve both to increase the knowledge base in the community regarding the fundamental properties and spectroscopic signatures of n-type doped SWNTs and to expand the versatility of functional SWNT network electrodes that have typically been resigned to high work function p-type SWNTs.

RESULTS AND DISCUSSION

Amine-Doped Transparent Conducting Films. We produced thin nanotube films by ultrasonic spraying of SWNTs dispersed in sodium carboxymethyl cellulose (CMC). An interconnected SWNT network was formed by removal of CMC in a nitric acid treatment as previously described.[2] After CMC removal, the film is doped heavily p-type from the nitric acid soak. The film may be made intrinsic by soaking in 4 M hydrazine overnight in a helium glovebox and then exposing the film to air.[21] Further details are provided in the Methods section. We further treated these intrinsic films with four different amines (hydrazine, methylamine, ethylenediamine, and polyethylenimine) and compared their sheet resistances and transmittance spectra (Figure 1a) for insights into the relative doping abilities of the different amines. Injection of carriers by dopants, whether holes or electrons, quenches the optical transitions of SWNTs by emptying initial states or filling final states involved in these transitions.[22,23] Due to strong many-body interactions, optical absorption in SWNTs is dominated by excitonic transitions. In Figure 1a, these transitions are labeled S_{11} for the first transition in semiconducting SWNTs, M_{11} for the first transition in metallic SWNTs, and so on.[22,23] The amine-treated samples each have significantly quenched intensity for the semiconducting S_{11} optical transition (Figure 1a), which is a clear sign of a doping-induced Fermi level shift. Of the four amines, hydrazine had the lowest sheet resistance and most significant S_{11} quenching. It is well-documented that nitric acid lowers the Fermi level of SWNT networks by removal of π electron density,[23,24] and conversely the data in Figure 1a suggest that adsorbed amine molecules and polymers increase the Fermi level by electron injection (*vide infra*).

For many device applications such as solar cells, touch screens, and LEDs,[2,3,6] it is important for SWNT thin films to have low sheet resistances while maintaining high visible light transmittance. Previous work has found that doping SWNT films p-type using nitric acid or thionyl chloride will drastically lower sheet resistance for films with relatively high transmittance,[21,24] allowing these films to be incorporated as hole-collecting electrodes in PV devices. To investigate how hydrazine compares to nitric acid, a series of films were sprayed of varying thickness and were doped either p-type with nitric acid or n-type with hydrazine. Figure 1b shows a plot of sheet resistance *versus* transmittance at 550 nm for these two series of films. We note that these transmittance values have been adjusted for the transmittance of the glass substrate, shown in Figure 1a, so that the values represent the percentage of light transmitted through the SWNT films only. This correction was done in order to provide values for useful comparison to other literature values

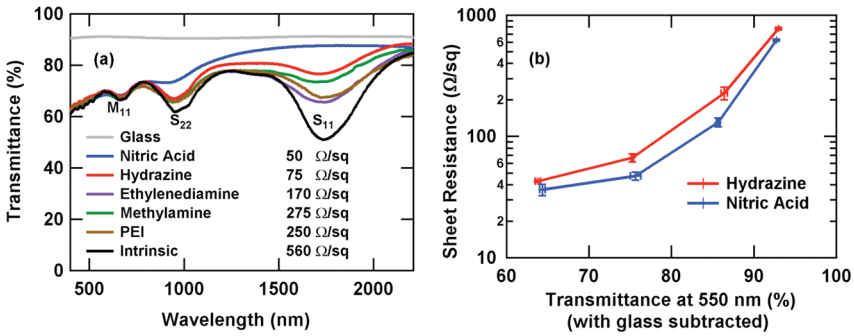

Figure 1. (a) Transmittance spectra of thin SWNT films of similar thickness treated with different dopants. The sheet resistance for each sample is noted, and a spectrum for the uncoated glass substrate is shown for comparison. Four different amines were tested with hydrazine showing the best quenching of the S_{11} transition and having the lowest sheet resistance. (b) Sheet resistance *vs* transmittance at 550 nm (T_{550}, with the glass substrate subtracted out) for a series of SWNT films. The films were sprayed at four different thicknesses and treated with either nitric acid or hydrazine. Sheet resistance for hydrazine films was measured in an inert atmosphere glovebox where they were prepared, while nitric-acid-treated samples were measured in air.

because this is the most common method of comparison found in the literature. Figure 1b demonstrates that hydrazine can be used to produce SWNT films with comparable sheet resistances, at a given transmittance, to those treated with HNO_3. This reduction in sheet resistance, along with bleaching of the S_{11} transition, is strong evidence that hydrazine acts as a chemical dopant. Furthermore, the performance demonstrated by Figure 1b is among the best ever obtained for p-type SWNT TCFs[25−27] (~50 Ω/sq at 75% T_{550}) and is the only result we are aware of demonstrating highly conductive n-type SWNT TCFs (~70 Ω/sq at 75% T_{550}).

The absorbance and transport measurements shown in Figure 1 demonstrate that small molecule and polymeric amines act as strong chemical dopants on single-walled carbon nanotubes, enabling highly conductive TCFs. However, these results cannot confirm that the amines are acting as n-type dopants since absorbance quenching can result from state-filling by holes or electrons. Furthermore, the M_{11} transitions are not affected in Figure 1, making it unclear to what extent the amines interact with metallic SWNTs. Finally, Figure 1 yields no information on the *mechanism* of amine interaction with the SWNT surface, that is, whether or not the amine molecules form covalent bonds with the SWNT or are simply physisorbed to the SWNT surface. To investigate these questions in more detail, we performed a variety of spectroscopic characterizations, including X-ray photoelectron spectroscopy (XPS), Raman spectroscopy, and nuclear magnetic resonance (NMR) spectroscopy.

X-ray Photoelectron Spectroscopy (XPS). Photoelectron spectroscopy is a useful tool for understanding molecular adsorption and charge transfer on SWNT surfaces. Since XPS probes the binding energy of core electrons, it is sensitive to changes in the Fermi level and can also be used to reveal the specific bonding environment(s) of carbon atoms in the doped SWNTs. Moreover, by comparing the intensities of different atomic core levels, the overall atomic composition can be determined, which can yield information on the coverage of dopants on the SWNT surface. Figure 2 displays core-level XPS spectra for intrinsic, hydrazine-doped, and nitric-doped SWNT buckypapers in the C 1s and N 1s regions. Significant doping-induced changes were observed in both the C 1s and N 1s core levels. Previously reported results for C 1s peak position in nitric-acid-treated samples were found to be shifted 0 eV,[25] 0.1 eV,[26] and 0.2 eV[28] toward lower binding energy compared to as-prepared samples. Since the binding energy is measured with respect to the Fermi level, a change in binding energy for the C 1s peak directly corresponds to a change in the Fermi level for the doped SWNTs. As shown in Figure 2a, we find a downshift of 0.1 eV, in good agreement with the previous results and consistent with a shift in the Fermi level toward the valence band edge due to p-type doping by HNO_3.[28] For the hydrazine-treated sample, we find an *upshift* of 0.7 eV in the C 1s binding energy, which is consistent with a sizable Fermi level shift toward the vacuum level. Importantly, the magnitude of this shift, 0.7 eV, is larger than the expected energy difference (ΔE_{LUMO}) between the Fermi level for intrinsic SWNTs and the first van Hove singularities for ~1.35 nm diameter semiconducting SWNTs. Taking the S_{11} energy of ~0.73 eV (S_{11} peak in Figure 1a of 1700 nm) as the average energy of the first excitonic transition, and an estimate of 0.25 eV as the approximate binding energy for this transition for 1.35 nm diameter SWNTs,[29] we approximate ΔE_{LUMO} to be 0.48 eV. Thus, the Fermi level shift of 0.7 eV demonstrates that N_2H_4 injects a sufficient electron density into the SWNT network to raise the Fermi level well into the conduction band of the semiconducting SWNTs.

The N 1s spectra were examined to determine the nitrogen bonding configurations present in nitric acid and hydrazine-treated samples. The as-prepared and

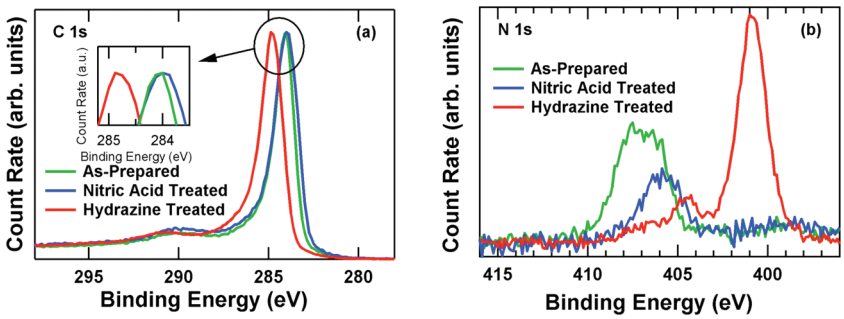

Figure 2. XPS spectra of (a) C 1s (normalized) and (b) N 1s (normalized to C 1s peak) core levels for as-prepared, nitric-acid-treated, and hydrazine-treated buckypapers.

nitric-doped samples both have peaks in the 406−407 eV range, consistent with HNO_3 and NO_2. The presence of this signal in the intrinsic sample indicates an incomplete removal of nitrate in the washing procedure used for SWNT purification. The N 1s spectrum of the hydrazine-treated sample shows a peak at 400.9 eV, which we attribute to hydrazine since it falls within the expected range for amines of 399−401 eV.[30] Two other small peaks appear between 404.5 and 407 eV, which could be residual nitrites and nitrates. The relative area of the 400.9 eV N peak for the hydrazine-doped sample indicates that approximately 79% of the nitrogen comes from hydrazine. On the basis of this value and the atomic composition found *via* XPS, we can approximate a coverage of ∼1.84 hydrazine molecules for every 100 carbon atoms and accordingly a density of 6.92×10^{20} hydrazine molecules/cm^3. Taking the number of carbon atoms per nm of SWNT to be $119.7 \times d_{(n,m)}$, where $d_{(n,m)}$ is the diameter of the SWNT in nanometers, we find a coverage of approximately three hydrazine molecules per nanometer of SWNT.

On the basis of the higher conductivity and stronger quenching of optical transitions in HNO_3-doped films, we expected the downshift in the C 1s core level for nitric-acid-treated films (Figure 2a) to be similar in magnitude to, or higher than, the upshift in hydrazine-treated films. Furthermore, we would expect to see a higher nitrogen concentration for the nitric-treated film than is observed. We attribute this discrepancy to desorption of nitric acid while under vacuum during XPS measurements, as has been seen before.[28] Further evidence of HNO_3 desorption was found when measuring sheet resistance. When samples were brought into a glovebox, they were exposed to vacuum (<100 mTorr) in an antechamber. For nitric-treated samples exposed to vacuum in the antechamber, even for a matter of 3−5 min, we observed a significant increase in the sheet resistance relative to samples kept in air and not exposed to vacuum. After ∼5 min in vacuum, the resistance had increased by around 20%, while after 1 h, the resistance had doubled. In contrast, when N_2H_4-treated samples were exposed to vacuum, there was no noticeable change in sheet resistance, even for samples kept under vacuum for an hour. Collectively, these experiments demonstrate that adsorbed hydrazine is significantly more stable on the SWNT than nitric acid in a vacuum environment, explaining why we are able to observe a much larger Fermi level shift in the high-vacuum XPS experiment for the hydrazine-doped sample. However, we note that the XPS spectra for both hydrazine- and nitric-doped SWNTs do not show evidence of additional peaks (relative to the undoped sample) associated with sp^3 carbon, which are expected in the range of 285−290 eV.[31] Thus, it appears that the mechanism for SWNT doping is based on charge transfer from physically adsorbed dopant molecules without covalent bond formation, as we confirm by NMR measurements below.

Raman Spectroscopy. Raman spectroscopy provides further insight into the effects of doping on SWNT samples. For chemical dopants, charge transfer from electron donors into the SWNT π system softens the C−C bonds, leading to a red shift of Raman peaks, while charge transfer from the SWNT π system into electron acceptors stiffens the bonds and blue shifts Raman peaks.[12,26,32] The G and G′ bands are often used to investigate charge transfer in doped SWNTs.[26,33,34] For example, studies using Li, K, and Rb as electron donors have found doping-induced red shifts of up to 8 cm^{-1} in the G band due to electron transfer into the nanotubes.[12,13,32] In contrast, for electron acceptors like HNO_3 and Br_2, *blue shifts* are observed for both the G and G′ peaks.[26,32] Shin *et al.* investigated p-doped arc discharge nanotubes treated with HNO_3 and report blue shifts of 9.9 cm^{-1} in the G′ band when excited with a 1.96 eV laser, which mainly probes the metallic SWNTs and blue shifts of 21.6 cm^{-1} for the G′ band with a 1.58 eV laser, which primarily excites semiconducting SWNTs.[26] Other complexities exist for metallic SWNTs. For example, the G$^-$ component of the metallic G band stiffens for both electron and hole injection, because of strong electron-phonon coupling for this mode.

While photoabsorption and XPS measurements demonstrate that hydrazine raises the Fermi level into the conduction band of the semiconducting SWNTs, these measurements do not address the scope of

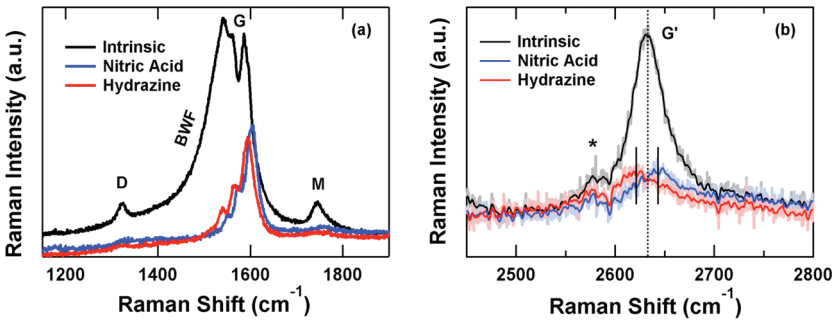

Figure 3. (a) Raman spectra of G bands for thin SWNT films of different doping types: intrinsic (black), nitric-doped (blue), and hydrazine-doped (red). The hydrazine- and nitric-treated films have a doping-induced reduction of the BWF line shape as compared to the intrinsic film, as well as a significant reduction in D and M bands. (b) Raman spectra of G′ band for the same films show doping-induced shifts. The asterisk indicates background from the substrate and sample holder. Excitation is at 1.96 eV (632.8 nm), primarily resonant with metallic SWNTs.

interaction with metallic SWNTs. To probe metallic nanotubes, we took Raman spectra using an excitation laser of 1.96 eV (632.8 nm), which is resonant with the M_{11} transition of 1.35 nm diameter SWNTs. In Figure 3a, the G bands for three samples of different doping (intrinsic, n-type with hydrazine, and p-type with nitric acid) are shown. We observe a significant reduction of the asymmetric Breit−Wigner−Fano (BWF) line shape of the G band for metallic SWNTs in the hydrazine- and nitric-treated samples, which is consistent with previous work on HNO_3- and $SOCl_2$-treated SWNTs that attribute this decrease to a loss of continuum states due to doping.[26,35] We further find that both the D (~1320 cm^{-1}) and M (~1745 cm^{-1}) bands in the two doped samples are greatly reduced as compared to the intrinsic film (Figure 3a). The complexity of the G band at this excitation wavelength makes the determination of absolute doping-induced shift (ΔG) difficult. However, we note that the G band for the hydrazine-doped sample is red-shifted 8.8 cm^{-1} relative to the nitric-doped sample, as expected for samples that are relatively electron-rich and electron-poor, respectively. The structure of the G′ band at ~2630 cm^{-1} is less complex than that of the G band, and the G′ position has been shown to be very sensitive to charge transfer doping of SWNTs. Figure 3b shows the G′ band for the same three samples, showing dramatic quenching of the G′ for both N_2H_4 and HNO_3. Furthermore, Figure 3b demonstrates a red shift for the hydrazine-doped sample of approximately 11.8 cm^{-1} and a blue shift of 10.4 cm^{-1} for the nitric-doped sample. Since shifts in opposite directions are expected for the injection of holes and electrons, these results confirm the conclusion reached through XPS measurements that hydrazine dopes the SWNTs strongly n-type by injecting electrons and raising the Fermi level toward vacuum.

Nuclear Magnetic Resonance (NMR). Solid-state ^{13}C nuclear magnetic resonance (NMR) spectroscopy with magic-angle spinning (MAS) is a powerful tool for probing the local chemical and electronic environment of carbon nuclei in SWNTs. While the benefits of NMR for studying functionalized SWNTs[31,36] are widely appreciated due to the obvious tie to traditional aromatic substitution reactions, NMR is also particularly useful for studying charge-transfer-induced changes in the Fermi level.[37] The observed chemical shift (δ) for ^{13}C nuclei can be separated into two parts, the chemical shift (σ) and the Knight shift (K):

$$\delta = \sigma + K \quad (1)$$

In eq 1, σ and K are second-rank tensors and consist of an isotropic and anisotropic part. The chemical shift σ arises from two primary contributions—so-called London ring currents due to delocalized interatomic currents in the aromatic ring structure, and the intra-atomic "Pople" contribution arising from the hybridization of the carbon atom. The Knight shift K arises from short- (isotropic) or long-distance (anisotropic) coupling of nuclear spins to the spins of conduction electrons. The isotropic Knight shift (K_{iso}) is paramagnetic (causing a shift to *higher frequency*) and is related to the Fermi contact between nuclei and conduction electrons in orbitals with non-negligible s character. Thus, K_{iso} is proportional to the probability density of conduction electrons at the nucleus $\Psi_F(0)^2$ and the density of states at the Fermi level $n(E_F)$:

$$K_{iso} = \frac{8\pi}{3}\psi_F(0)^2\mu_B^2 n(E_F) \quad (2)$$

where μ_B is the Bohr magneton. In graphite, $\Psi_F(0)^2$ is negligible because conduction electrons only occupy orbitals with p character. However, curvature-induced sp^2-sp^3 rehybridization in SWNTs and fullerenes leads to a non-negligible s character for conduction electrons, meaning Fermi level changes due to charge transfer should induce an isotropic Knight shift.[37,38]

Figure 4a shows solid-state MAS ^{13}C NMR spectra for the same SWNT sample either in an intrinsic, n-type, or p-type state. For each doped sample, the $^1H-^{13}C$ cross-polarization (CP-MAS) NMR spectrum is also shown. In each case (n- and p-type state), the transfer of magnetization from protons of the dopant species to adjacent ^{13}C nuclei on the SWNT was observed.

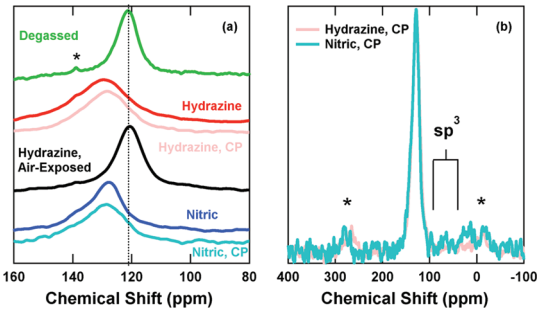

Figure 4. (a) Solid-state MAS ^{13}C NMR spectra of 20% ^{13}C-enriched SWNT sample with 66% s-SWNTs after various treatments (listed above/below the corresponding spectra). $^{1}H-^{13}C$ CP-MAS spectra are labeled accordingly. The asterisk indicates the ^{13}C resonance from the polyethylene plugs used to balance the rotor. (b) Comparison of CP-MAS NMR spectra for hydrazine- and nitric-doped samples, highlighting the area where peaks are expected for sp^3 carbon. Spinning side bands are labeled with asterisks.

The series of spectra in Figure 4a demonstrates several interesting trends. The isotropic chemical shift for the intrinsic SWNT sample, directly after degassing, is 121 ppm, the characteristic chemical shift expected for undoped, highly pure SWNTs.[39−41] Upon n-type doping the SWNT sample with hydrazine, the peak shifts to higher frequency by 8 ppm and broadens significantly relative to the undoped SWNT sample.[42] The CP-MAS spectrum for the same n-type SWNT sample shows a similar broad and shifted peak at 128 ppm. After exposing the n-type sample to air for several hours, the peak narrows and shifts back to its original position at 121 ppm. Finally, when the sample is doped p-type by soaking in concentrated nitric acid, the peak again shifts to higher frequency (128−129 ppm) and broadens significantly, a strikingly similar behavior to the n-type doped SWNT sample.[42] Figure 4b compares the CP-MAS spectra for the hydrazine- and nitric-doped SWNTs. The isotropic chemical shift of SWNTs, in the range of 121 ppm (128 ppm for the doped samples), is due to sp^2-hybridized carbon atoms. When aromatic sp^2 systems such as fullerenes or nanotubes are converted to sp^3 through the formation of covalent bonds, new peak(s) appear at lower frequency for the sp^3 carbon nuclei, typically in the range of 50−90 ppm.[31,43] Figure 4b shows a complete lack of sp^3-related peaks in the spectra for both hydrazine- and nitric-doped SWNTs. This result clearly demonstrates that the mechanism for doping involves physically adsorbed dopant molecules and no covalent bond formation, in agreement with the conclusions reached from XPS analysis.

Returning to eq 2, the significant paramagnetic shifts observed for the ^{13}C resonance in doped SWNT samples are consistent with Knight shifts arising from a substantial increase in the density of states at the Fermi level due to injection of electrons or holes from the physisorbed dopants. This conclusion is consistent with the absorbance, Raman, and XPS measurements discussed above and lends further support to strong charge transfer interactions of SWNTs with amines such as hydrazine that result in injection of electrons into the SWNTs. The 7−8 ppm paramagnetic shift observed for the nitric-acid-doped SWNTs is also consistent with our previous work on SWNTs doped strongly p-type with sulfuric acid.[39] The efficiency of the spin polarization transfer process utilized in the CP-MAS experiment is distance-dependent, with a $1/r^6$ dependence. Thus, CP-MAS NMR can selectively probe SWNT ^{13}C nuclei in direct proximity of absorbed dopant molecules. In both cases, for hydrazine- and nitric-acid-doped samples, the CP-MAS spectra are similar in chemical shift and line width to the equivalent MAS ^{13}C NMR spectra, implying a rather complete intercalation and coverage of the dopant molecules into the SWNT buckypapers. Finally, the spectrum of the hydrazine-treated air-exposed sample confirms that reaction of the hydrazine sample in air over the course of several hours returns the doped SWNTs to its intrinsic state and is completely reversible.[44]

It is interesting to compare these results to previous results on other charge-transfer-doped graphite-based systems. Significant Knight shifts have been consistently observed for *electron-doped* graphitic systems such as alkali-doped graphite intercalation compounds (GIC),[45−47] C_{60} compounds,[48] and SWNTs.[37] However, these shifts (Knight) have not been observed in *hole-doped* GICs,[49] a phenomenon that has spawned much discussion in the GIC community.[50] NMR measurements on both oxidized and reduced C_{60} have demonstrated doping-induced paramagnetic shifts that are accompanied by broadening, although the observed shifts for the oxidized fullerene are smaller than their reduced counterparts.[43,48] Importantly, our results demonstrate that the coupling of ^{13}C nuclear spins to the spins of both free electrons in n-type SWNTs or free holes in p-type SWNTs induces a paramagnetic shift (of similar magnitude) in the aromatic ^{13}C NMR resonance for intrinsic SWNTs. To equate the magnitude of the NMR shift to a density of injected carriers, a rigorous treatment would take into account the temperature-dependent spin−lattice relaxation time, which can be related directly to $n(E_F)$ *via* the Korringa relation,[51] but this is beyond the scope of this article.

Air Stability of Amine n-Type Doping. Now that we have rigorously characterized the n-type doping effects of amine molecules on SWNT networks, we return to a practical consideration for device applications. A shortcoming of nearly all strategies for producing n-type SWNTs is the lack of air stability. In an attempt to probe the air stability of our amine-doped n-type SWNT TCFs, we monitored the doping-induced S_{11} absorbance quenching for several different films. As shown in Figure 5a, we find that the doping effects of hydrazine are not stable in air for prolonged periods of time. By

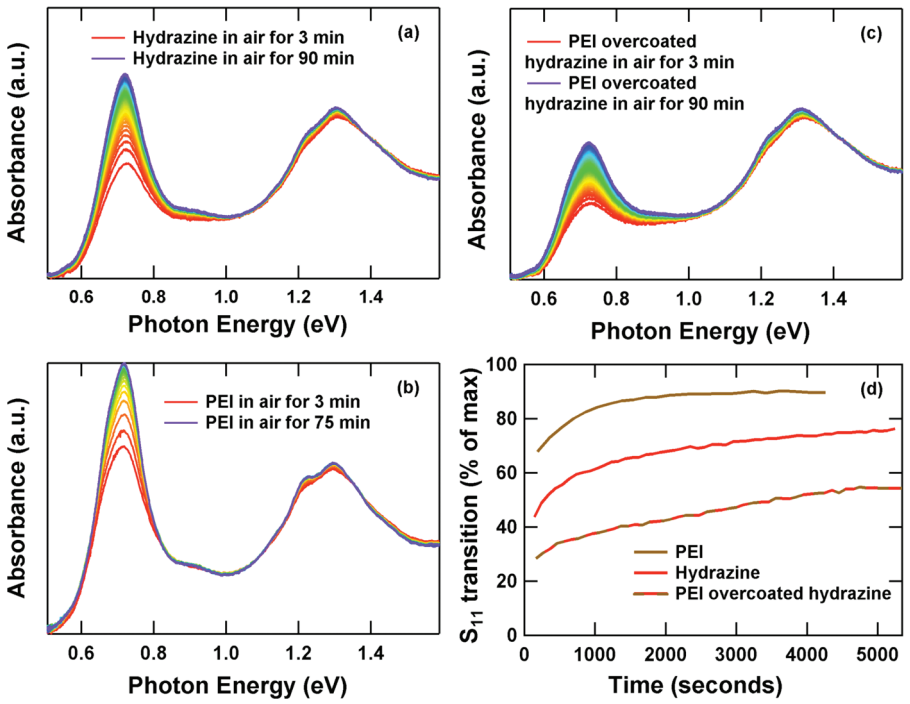

Figure 5. Time-dependent absorption of SWNT films in air after being treated with (a) hydrazine, (b) 10% w/v PEI (M_n = 10 000) in methanol, and (c) hydrazine and then overcoated with 27% w/v PEI (M_n = 600) in methanol. Spectra in (a−c) are taken every 2−3 min. (d) Time evolution of the integrated optical density of the S_{11} transition band is given as a percentage of the full value (seen for an intrinsic sample) for each of the three films. Time 0 is approximate for each.

monitoring the strength of the S_{11} optical transition over time as the sample sits in air, we can see that the peak increases in strength with time as in Figure 5a, indicating a time-dependent de-doping of the film. This change in absorption is accompanied by an increase in sheet resistance, which is another indication that the doping level has decreased. This change in doping may be a result of hydrazine reacting in air,[52] compensation by a p-type dopant such as oxygen, desorption of hydrazine, or a combination of some of these processes. From our testing of samples in vacuum, described above, it appears unlikely that hydrazine desorption is the cause. We further find that returning a sample to an inert atmosphere after brief exposure to air partially quenches the S_{11} transition again and reduces the sheet resistance (see Supporting Information). As there is no additional dopant added by allowing a sample to sit in the helium glovebox, this apparent "re-doping" is consistent with a decrease in compensation *via* oxygen desorption from the SWNT film while remaining in a glovebox or when in vacuum as the sample is brought inside. However, after prolonged exposure to air, recovery of n-type conductivity is no longer possible.

To address stability issues, several groups have explored the use of the amine-containing polymer polyethylenimine (PEI), which has been used to produce n-type FETs.[17,53] We performed a series of experiments to probe and compare the air stability of our hydrazine- and PEI-doped SWNT TCFs. Films treated with PEI were found to partially quench the S_{11} optical transition with sheet resistances several times higher than comparable hydrazine-treated films (Figure 1). After exposure to air, we found that the PEI-treated films also showed signs of decreased doping, indicated by a time-dependent increase in sheet resistance and the return of the S_{11} (Figure 5b). We speculate that part of the reason that PEI has shown air-stable results in FETs[17] is due to its ability to keep oxygen away from the nanotubes. To investigate this further, we immersed a SWNT film, which had already been treated with hydrazine, in PEI. This film had a sheet resistance around half that of a sample treated solely with PEI. In Figure 5c, we show that the S_{11} transition returns much more slowly than for the other films treated with only hydrazine or PEI. In fact, the degree of S_{11} quenching after 90 min of air exposure is nearly equivalent to the quenching observed for the hydrazine-treated sample immediately after air exposure. It should be noted, however, that the results in Figure 5 are indicative of the best air stability achieved and that there can be significant variability between samples, as well as variations depending on the type of PEI used (see Supporting Information). This demonstration of improved air stability is promising and could be improved upon by optimization of the PEI overcoating, suggesting potential strategies to further develop air-stable n-type SWNT networks. Ultimately, for n-type SWNT networks to be adopted in technological applications such as photovoltaics, significantly improved stability over what is presented here will be necessary.[54]

CONCLUSIONS

In conclusion, four different amines (hydrazine, methylamine, ethylenediamine, and polyethylenimine) were used to treat thin conducting carbon nanotube networks. We found that all four amines induced a reduction in sheet resistance and partially quenched the S_{11} optical transition, as compared to intrinsic films, showing signs of n-type doping. n-Type TCFs, prepared from hydrazine-doped SWNT networks, performed nearly as well as their p-type counterparts with R_s values of 70 Ω/sq at T_{550} of 75%. Hydrazine-doped SWNTs were studied in depth to ascertain the fundamental spectroscopic signatures of n-type SWNTs and compare them to those of a well-characterized p-type dopant. Hydrazine-induced spectroscopic changes clearly demonstrate the n-type doping behavior, as deduced by an upshift in the XPS-measured C 1s core-level binding energies, indicating an increase in the Fermi level toward the vacuum level. Furthermore, we observed red shifts in Raman bands due to injected charge from the hydrazine electron donor, an opposite shift to that observed for p-type SWNTs doped by nitric acid. NMR results demonstrate that n- and p-type doping of SWNTs leads to significant paramagnetic shifts in the isotropic ^{13}C chemical shift. Because n-type SWNTs generally lack the air stability of their p-type counterparts, we investigated the use of a polymer amine for our macroscopic thin film networks that has seen some success for FETs and single-tube studies. Although PEI did not display doping characteristics as favorable as hydrazine, it was successful at prolonging the stability of our hydrazine-doped n-type film in air, suggesting potential strategies for the further development of air-stable n-type SWNT networks. n-Type SWNT TCFs, such as the ones developed here, offer the ability to create efficient photovoltaic devices and LEDs with transparent SWNTs as both cathode and anode, and could potentially enable tandem devices which require transparent electrodes for both contacts. Furthermore, spatially controlled coating of SWNT networks (or forests) with amines as n-type dopants, in conjunction with molecular p-type dopants, opens up the possibility for macroscale p−n junction photovoltaics.

METHODS

Synthesis, purification, and ultrasonic spraying of CMC-dispersed SWNTs techniques employed in this paper have been described previously.[2,24] CMC was removed by overnight soaking of the films in 4 M nitric acid, which collapses the isolated SWNTs into an interconnected conducting network as well as serves to dope them p-type. These TCFs were used in absorption, four-point probe, and Raman measurements.

To remove the doping effects of the nitric acid treatment and create intrinsic films, the sample was immersed in either 1 or 4 M hydrazine in a helium environment and then exposed to air. Doping the films n-type involved a two-step process from the nitric-doped samples. First, the films were immersed in 4 M hydrazine and then exposed briefly to air (<10 min). Next, the films were immersed in neat hydrazine and kept in an inert environment. Soaking times for 1 and 4 M hydrazine lasted from 4 to 24 h, while neat hydrazine was only used for about 4 h.

For the small molecule amine comparison, we started with intrinsic samples and soaked the films overnight in a glovebox in either hydrazine (neat), ethylenediamine (neat), or methylamine (33 wt % in ethanol). For PEI-treated samples shown, intrinsic films were immersed in 10% w/v PEI (Aldrich, M_n = 10 000) in methanol overnight, followed by rinsing in methanol to match previous work on PEI.[55] For PEI used to overcoat hydrazine in Figure 5, we used 27% w/v PEI (Aldrich, M_n = 600) in methanol overnight with rinsing.

Sheet resistance measurements were taken on a linear four-point probe.[56] Hydrazine (and other amine)-treated films were tested with a probe in the glovebox where they were prepared, while nitric-treated samples were tested in air. Nitric-treated samples that were brought into the glovebox had higher sheet resistances because of significant desorption of the dopant during the vacuum exposure. Raman spectroscopy was performed using a Jobin Yvon 270 M spectrometer with a HeNe excitation laser at 1.96 eV (632.8 nm) in a backscattering configuration. The optical absorption spectra were taken on a Varian Cary 500 spectrometer.

For XPS and NMR measurements, thicker "buckypapers" were used instead of sprayed films. The SWNTs for NMR were synthesized *via* laser vaporization as above but used a 20% ^{13}C-enriched graphite target. The ^{13}C-enriched SWNTs were subjected to density gradient ultracentrifugation to separate SWNTs by electronic structure and remove residual catalyst metal (Co, Ni) impurities for the NMR measurements. Several samples were combined to produce a sample with ~66% semiconducting SWNTs, as measured by absorbance spectroscopy, after which a buckypaper was produced by vacuum filtration. This sample was degassed by heating to 200 °C on a temperature-programmed desorption apparatus to remove adsorbed impurities before doping. The buckypaper for XPS measurements was formed from unenriched (*i.e.*, no ^{13}C) laser vaporization SWNT sample that was subjected to our typical purification. This involves refluxing in nitric acid for 18 h, and then filtering and washing with water, acetone, and NaOH remove impurities generated by the reflux. This buckypaper was then burned rapidly (30 s) in air at 525 °C to remove amorphous carbon.

NMR samples were prepared in a glovebox under a helium atmosphere. The SWNT materials (~0.8 mg) were loaded into zirconia rotors (7 mm outer diameter) and packed between two plugs of either polyethylene or Teflon to balance the rotor, center the small amount of SWNT sample in the NMR coil, and provide a barrier against exposure to ambient conditions. Polyethylene plugs were used in single pulse experiments (35 000 scans) and Teflon plugs in CP experiments (150 000 scans) in order to minimize background signals. Samples were transferred in a helium bag directly to the NMR spectrometer. High-resolution, solid-state ^{13}C NMR spectra were collected on a Bruker Avance 200 MHz spectrometer (4.7 T) operating at 50.13 MHz for ^{13}C at room temperature, with a MAS rotation rate of 7 kHz under a nitrogen atmosphere. The spectra were acquired under high-power proton decoupling using a $\pi/2$ pulse length of 5.3 μs and a recycle delay of 10 s and were referenced to adamantane. The features at 115 and 139 ppm are due to unsaturated impurities in the polyethylene plugs. Ramped-amplitude CP experiments were carried out at room temperature using a 5 ms contact time, spinning rate of 7 kHz, and a pulse repetition rate of 1.0 s.

Acknowledgment. We thank Ross Larsen for density functional calculations, and for the table of contents image. Doping and spectroscopy studies were supported by the Solar Photochemistry program of the U.S. Department of Energy, Office of

Science, Basic Energy Sciences, Division of Chemical Sciences, Geosciences and Biosciences, under Contract No. DE-AC36-08GO28308 to NREL. Thin film development was supported by the Seed Fund program of the Solar Energy Technology Program (SETP).

Supporting Information Available: Additional experimental details. This material is available free of charge *via* the Internet at http://pubs.acs.org.

REFERENCES AND NOTES

1. Avouris, P. Carbon Nanotube Electronics. *Chem. Phys.* **2002,** *281*, 429–445.
2. Tenent, R. C.; Barnes, T. M.; Bergeson, J. D.; Ferguson, A. J.; To, B.; Gedvilas, L. M.; Heben, M. J.; Blackburn, J. L. Ultrasmooth, Large-Area, High-Uniformity, Conductive Transparent Single-Walled-Carbon-Nanotube Films for Photovoltaics Produced by Ultrasonic Spraying. *Adv. Mater.* **2009,** *21*, 3210–3216.
3. Barnes, T. M.; Bergeson, J. D.; Tenent, R. C.; Larsen, B. A.; Teeter, G.; Jones, K. M.; Blackburn, J. L.; van de Lagemaat, J. Carbon Nanotube Network Electrodes Enabling Efficient Organic Solar Cells without a Hole Transport Layer. *Appl. Phys. Lett.* **2010,** *96*, 243309-3.
4. Ou, E. C. W.; Hu, L.; Raymond, G. C. R.; Soo, O. K.; Pan, J.; Zheng, Z.; Park, Y.; Hecht, D.; Irvin, G.; Drzaic, P.; *et al.* Surface-Modified Nanotube Anodes for High Performance Organic Light-Emitting Diode. *ACS Nano* **2009,** *3*, 2258–2264.
5. Zhou, Y.; Gaur, A.; Hur, S.-H.; Kocabas, C.; Meitl, M. A.; Shim, M.; Rogers, J. A. p-Channel, n-Channel Thin Film Transistors and p−n Diodes Based on Single Wall Carbon Nanotube Networks. *Nano Lett.* **2004,** *4*, 2031–2035.
6. Aguirre, C. M.; Auvray, S.; Pigeon, S.; Izquierdo, R.; Desjardins, P.; Martel, R. Carbon Nanotube Sheets as Electrodes in Organic Light-Emitting Diodes. *Appl. Phys. Lett.* **2006,** *88*, 183104-3.
7. van de Lagemaat, J.; Barnes, T. M.; Rumbles, G.; Shaheen, S. E.; Coutts, T. J.; Weeks, C.; Levitsky, I.; Peltola, J.; Glatkowski, P. Organic Solar Cells with Carbon Nanotubes Replacing In_2O_3:Sn as the Transparent Electrode. *Appl. Phys. Lett.* **2006,** *88*, 233503.
8. Yu, Z.; Hu, L.; Liu, Z.; Sun, M.; Wang, M.; Gruner, G.; Pei, Q. Fully Bendable Polymer Light Emitting Devices with Carbon Nanotubes as Cathode and Anode. *Appl. Phys. Lett.* **2009,** *95*, 203304-3.
9. Zhou, C.; Kong, J.; Yenilmez, E.; Dai, H. Modulated Chemical Doping of Individual Carbon Nanotubes. *Science* **2000,** *290*, 1552–1555.
10. Lee, J.; Gipp, P.; Heller, C. Carbon Nanotube p−n Junction Diodes. *Appl. Phys. Lett.* **2004,** *85*, 145.
11. Penicaud, A.; Poulin, P.; Derre, A.; Anglaret, E.; Petit, P. Spontaneous Dissolution of a Single-Wall Carbon Nanotube Salt. *J. Am. Chem. Soc.* **2004,** *127*, 8–9.
12. Claye, A.; Nemes, N.; Janossy, A.; Fischer, J. E. Structure and Electronic Properties of Potassium-Doped Single-Wall Carbon Nanotubes. *Phys. Rev. B* **2000,** *62*, R4845–R4848.
13. Claye, A.; Rahman, S.; Fischer, J. E.; Sirenko, A.; Sumanasekera, G.; Eklund, P. C. *In Situ* Raman Scattering Studies of Alkali-Doped Single Wall Carbon Nanotubes. *Chem. Phys. Lett.* **2001,** *333*, 16–22.
14. Takenobu, T.; Takano, T.; Shiraishi, M.; Murakami, Y.; Ata, M.; Kataura, H.; Achiba, Y.; Iwasa, Y. Stable and Controlled Amphoteric Doping by Encapsulation of Organic Molecules Inside Carbon Nanotubes. *Nat. Mater.* **2003,** *2*, 683–688.
15. Koizhaiganova, R. B.; Hwang, D. H.; Lee, C. J.; Roth, S.; Dettlaff-Weglikowska, U. n-Type Doping Effect of Single-Walled Carbon Nanotubes with Aromatic Amines. *Phys. Status Solidi B* **2010,** *247*, 2793–2796.
16. Klinke, C.; Chen, J.; Afzali, A.; Avouris, P. Charge Transfer Induced Polarity Switching in Carbon Nanotube Transistors. *Nano Lett.* **2005,** *5*, 555–558.
17. Shim, M.; Javey, A.; Kam, N. W.; Dai, H. Polymer Functionalization for Air-Stable n-Type Carbon Nanotube Field-Effect Transistors. *J. Am. Chem. Soc.* **2001,** *123*, 11512–11513.
18. Tung, V. C.; Chen, L.-M.; Allen, M. J.; Wassei, J. K.; Nelson, K.; Kaner, R. B.; Yang, Y. Low-Temperature Solution Processing of Graphene−Carbon Nanotube Hybrid Materials for High-Performance Transparent Conductors. *Nano Lett.* **2009,** *9*, 1949–1955.
19. Wang, C.; Ryu, K.; Badmaev, A.; Patil, N.; Lin, A.; Mitra, S.; Wong, H.-S. P.; Zhou, C. Device Study, Chemical Doping, and Logic Circuits Based on Transferred Aligned Single-Walled Carbon Nanotubes. *Appl. Phys. Lett.* **2008,** *93*, 033101.
20. Casterman, D.; De Souza, M. Effect of Hydrazine on Al-Contacted Carbon Nanotube Field Effect Transistors Using Density Functional Theory. *J. Sci. Conf. Proc.* **2009,** *1*, 24–28.
21. Barnes, T. M.; Blackburn, J. L.; van De Lagemaat, J.; Coutts, T. J.; Heben, M. J. Reversibility, Dopant Desorption, and Tunneling in the Temperature-Dependent Conductivity of Type-Separated, Conductive Carbon Nanotube Networks. *ACS Nano* **2008,** *2*, 1968–1976.
22. Kazaoui, S.; Minami, N.; Jacquemin, R.; Kataura, H.; Achiba, Y. Amphoteric Doping of Single-Wall Carbon-Nanotube Thin Films As Probed by Optical Absorption Spectroscopy. *Phys. Rev. B* **1999,** *60*, 13339–13342.
23. Zhou, W.; Vavro, J.; Nemes, N.; Fischer, J.; Borondics, F.; Kamarás, K.; Tanner, D. Charge Transfer and Fermi Level Shift in p-Doped Single-Walled Carbon Nanotubes. *Phys. Rev. B* **2005,** *71*, 1–7.
24. Blackburn, J. L.; Barnes, T. M.; Beard, M. C.; Kim, Y.-H.; Tenent, R. C.; McDonald, T. J.; To, B.; Coutts, T. J.; Heben, M. J. Transparent Conductive Single-Walled Carbon Nanotube Networks with Precisely Tunable Ratios of Semiconducting and Metallic Nanotubes. *ACS Nano* **2008,** *2*, 1266–1274.
25. Geng, H.-Z.; Kim, K. K.; So, K. P.; Lee, Y. S.; Chang, Y.; Lee, Y. H. Effect of Acid Treatment on Carbon Nanotube-Based Flexible Transparent Conducting Films. *J. Am. Chem. Soc.* **2007,** *129*, 7758–7759.
26. Shin, D.-W.; Lee, J. H.; Kim, Y.-H.; Yu, S. M.; Park, S.-Y.; Yoo, J.-B. A Role of HNO_3 on Transparent Conducting Film with Single-Walled Carbon Nanotubes. *Nanotechnology* **2009,** *20*, 475703.
27. Wu, Z.; Chen, Z.; Du, X.; Logan, J. M.; Sippel, J.; Nikolou, M.; Kamaras, K.; Reynolds, J. R.; Tanner, D. B.; Hebard, A. F.;*et al.*Transparent, Conductive Carbon Nanotube Films. *Science* **2004,** *305*, 1273–1276.
28. Graupner, R.; Abraham, J.; Vencelova, A.; Seyller, T.; Hennrich, F.; Kappes, M. M.; Hirsch, A.; Ley, L. Doping of Single-Walled Carbon Nanotube Bundles by Brønsted Acids. *Phys. Chem. Chem. Phys.* **2003,** *5*, 5472–5476.
29. Dukovic, G.; Wang, F.; Song, D.; Sfeir, M. Y.; Heinz, T. F.; Brus, L. E. Structural Dependence of Excitonic Optical Transitions and Band-Gap Energies in Carbon Nanotubes. *Nano Lett.* **2005,** *5*, 2314–2318.
30. Ramanathan, T.; Fisher, F. T.; Ruoff, R. S.; Brinson, L. C. Amino-Functionalized Carbon Nanotubes for Binding to Polymers and Biological Systems. *Chem. Mater.* **2005,** *17*, 1290–1295.
31. Alemany, L. B.; Zhang, L.; Zeng, L.; Edwards, C. L.; Barron, A. R. Solid-State NMR Analysis of Fluorinated Single-Walled Carbon Nanotubes: Assessing the Extent of Fluorination. *Chem. Mater.* **2007,** *19*, 735–744.
32. Rao, A. M.; Eklund, P. C.; Bandow, S.; Thess, A.; Smalley, R. E. Evidence for Charge Transfer in Doped Carbon Nanotube Bundles from Raman Scattering. *Nature* **1997,** *388*, 257–259.
33. Dresselhaus, M.; Dresselhaus, G.; Saito, R.; Jorio, A. Raman Spectroscopy of Carbon Nanotubes. *Phys. Rep.* **2005,** *409*, 47–99.
34. Maciel, I. O.; Anderson, N.; Pimenta, M. A.; Hartschuh, A.; Qian, H.; Terrones, M.; Terrones, H.; Campos-Delgado, J.; Rao, A. M.; Novotny, L.; *et al.* Electron and Phonon Renormalization near Charged Defects in Carbon Nanotubes. *Nat. Mater.* **2008,** *7*, 878–883.

35. Dettlaff-Weglikowska, U.; Skákalová, V.; Graupner, R.; Jhang, S. H.; Kim, B. H.; Lee, H. J.; Ley, L.; Park, Y. W.; Berber, S.; Tománek, D.; *et al.* Effect of $SOCl_2$ Treatment on Electrical and Mechanical Properties of Single-Wall Carbon Nanotube Networks. *J. Am. Chem. Soc.* **2005,** *127*, 5125–5131.
36. Zeng, L.; Alemany, L.; Edwards, C.; Barron, A. Demonstration of Covalent Sidewall Functionalization of Single Wall Carbon Nanotubes by NMR Spectroscopy: Side Chain Length Dependence on the Observation of the Sidewall sp^3 Carbons. *Nano Res.* **2008,** *1*, 72–88.
37. Schmid, M.; Goze-Bac, C.; Krämer, S.; Roth, S.; Mehring, M.; Mathis, C.; Petit, P. Metallic Properties of Li-Intercalated Carbon Nanotubes Investigated by NMR. *Phys. Rev. B* **2006,** *74*, 073416.
38. Goze-Bac, C.; Latil, S.; Lauginie, P.; Jourdain, V.; Conard, J.; Duclaux, L.; Rubio, A.; Bernier, P. Magnetic Interactions in Carbon Nanostructures. *Carbon* **2002,** *40*, 1825–1842.
39. Engtrakul, C.; Davis, M. F.; Gennett, T.; Dillon, A. C.; Jones, K. M.; Heben, M. J. Protonation of Carbon Single-Walled Nanotubes Studied Using ^{13}C and $^{1}H-^{13}C$ Cross Polarization Nuclear Magnetic Resonance and Raman Spectroscopies. *J. Am. Chem. Soc.* **2005,** *127*, 17548–17555.
40. Engtrakul, C.; Davis, M. F.; Mistry, K.; Larsen, B. A.; Dillon, A. C.; Heben, M. J.; Blackburn, J. L. Solid-State ^{13}C NMR Assignment of Carbon Resonances on Metallic and Semiconducting Single-Walled Carbon Nanotubes. *J. Am. Chem. Soc.* **2010,** *132*, 9956–9957.
41. Our recent NMR study on SWNTs separated by electronic structure demonstrated that this peak can be deconvoluted into two peaks: a narrow (fwhm ~7−8 ppm) peak at ~121 ppm for s-SWNTs and a wider (fwhm ~15 ppm) peak at ~122−125 ppm for m-SWNTs.
42. The FT- and CP-MAS spectra of the doped (both n-type and p-type) are also best fit by two Lorentzian peaks. Although it is tempting to assign these two peaks to doped s- and m-SWNTs, the data shown do not allow us to draw this conclusion. We are currently studying the effects of these doping treatments on s- and m-SWNTs separated by electronic structure. These results are beyond the scope of this article and will be reported in a future paper.
43. Reed, C. A.; Kim, K.-C.; Bolskar, R. D.; Mueller, L. J. Taming Superacids: Stabilization of the Fullerene Cations HC_{60}^{+} and $C_{60}^{\cdot+}$. *Science* **2000,** *289*, 101–104.
44. We also note that the Raman and XPS signals for the hydrazine, air-exposed samples returned to the positions measured for intrinsic SWNTs.
45. Maniwa, Y.; Kume, K.; Suematsu, H.; Tanuma, S. High Resolution ^{13}C NMR in K-Graphite Intercalation Compounds-*c*-Axis Charge Distribution. *J. Phys. Soc. Jpn.* **1985,** *54*, 666–676.
46. Conrad, J.; Gutierrez-Le Brun, M.; Lauginie, P.; Estrade-Swarckopf, H.; Hermann, G. High Field ^{13}C NMR in Lamellar Compounds of Graphite and a Model of "In Plane Localized" Densities of States. *Synth. Met.* **1980,** *2*, 227–236.
47. Kume, K.; Nomura, K.; Hiroyama, Y.; Maniwa, Y.; Suematsu, H.; Tanuma, S. High Resolution ^{13}C NMR in GIC and *c*-Axis Charge Distribution. *Synth. Met.* **1985,** *12*, 307–312.
48. Maniwa, Y.; Sugiura, D.; Kume, K.; Kikuchi, K.; Suzuki, S.; Achiba, Y.; Hirosawa, I.; Tanigaki, K.; Shimoda, H.; Iwasa, Y. Determination of ^{13}C NMR Isotropic Knight Shift and Deviation from BCS Relation in A_3C_{60} Superconductors. *Phys. Rev. B* **1996,** *54*, R6861.
49. Conrad, J. *Phys. Colloq. No. 2 (Paris)* **1986,** *11*, 235.
50. Fretigny, C.; Saint Jean, M.; Quinton, M. F. Rigorous Calculation of the ^{13}C Orbital Shift in Graphite Intercalation Compounds. *Phys. Rev. B* **1994,** *49*, 9586–9593.
51. Schmid, M.; Goze-Bac, C.; Krämer, S.; Roth, S.; Mehring, M.; Mathis, C.; Petit, P. Metallic Properties of Li-Intercalated Carbon Nanotubes Investigated by NMR. *Phys. Rev. B* **2006,** *74*, 5–8.
52. *Hydrazine (Environmental Health Criteria)*; World Health Organization: Geneva, 1987.
53. Ham, M.-H.; Paulus, G. L. C.; Lee, C. Y.; Song, C.; Kalantar-Zadeh, K.; Choi, W.; Han, J.-H.; Strano, M. S. Evidence for High-Efficiency Exciton Dissociation at Polymer/Single-Walled Carbon Nanotube Interfaces in Planar Nano-heterojunction Photovoltaics. *ACS Nano* **2010,** *4*, 6251–6259.
54. Chandra, B.; Afzali, A.; Khare, N.; El-Ashry, M. M.; Tulevski, G. S. Stable Charge-Transfer Doping of Transparent Single-Walled Carbon Nanotube Films. *Chem. Mater.* **2010,** *22*, 5179–5183.
55. Shim, M.; Ozel, T.; Gaur, A.; Wang, C. Insights on Charge Transfer Doping and Intrinsic Phonon Line Shape of Carbon Nanotubes by Simple Polymer Adsorption. *J. Am. Chem. Soc.* **2006,** *128*, 7522–30.
56. Smits, F. M. Measurement of Sheet Resistivities with the Four-Point Probe. *The Bell System Technical Journal* **1958,** *37*, 711–718.